Institute of Paper Science and Technology
Atlanta, Georgia

IPST TECHNICAL PAPER SERIES

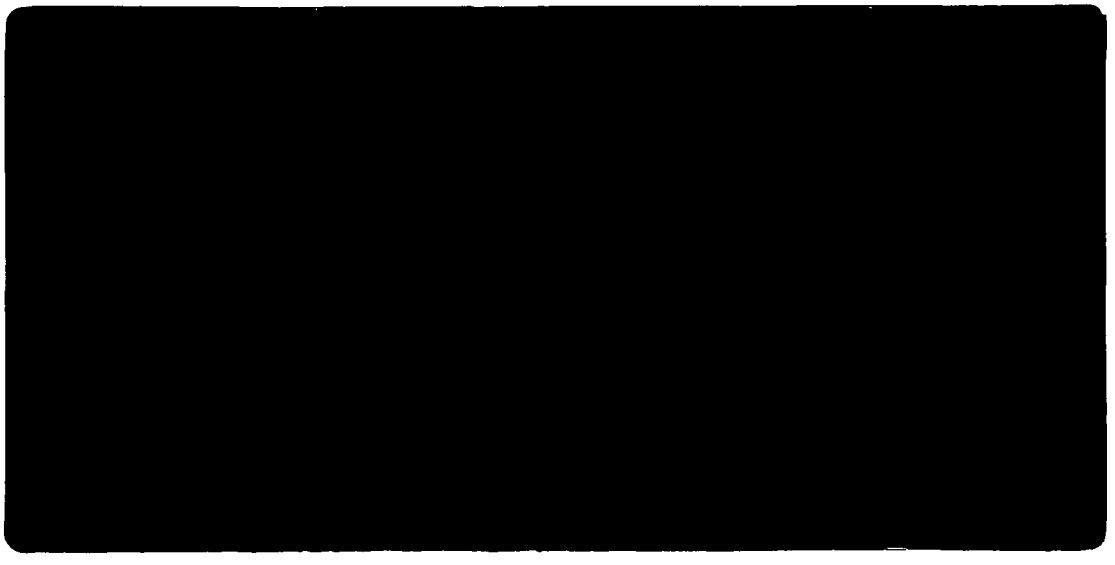

NUMBER 436

THE EFFECT OF RECOVERY FURNACE BULLNOSE DESIGNS ON UPPER FURNACE FLOW AND TEMPERATURE PROFILES

E.K. VAKKILAINEN, T.N. ADAMS, AND R.R. HORTON

APRIL 1992

The Effect of Recovery Furnace Bullnose Designs on Upper Furnace Flow and Temperature Profiles

E.K. Vakkilainen, T.N. Adams, and R.R. Horton

Submitted to
International Recovery Conference
June 7–11, 1992
Seattle, WA

The Effect of Recovery Furnace Bullnose Designs on Upper Furnace Flow and Temperature Profiles

Esa K. Vakkilainen, Terry N. Adams, and Robert R. Horton
Institute of Paper Science and Technology

ABSTRACT

A commercially available computational fluid dynamics code has been used to simulate temperature and flow profiles in the upper, convective heat transfer region of a recovery boiler for different bullnose designs. The convective heat transfer region of the furnace was simulated by examining a zone that begins below the bullnose and ends at the economizer. Superheater tubes and a boiler bank were included as internal wall boundaries in the problem description. A variety of inlet velocity profiles and temperature profiles were used to determine the sensitivity of the results to chosen inlet conditions. Results from this work show that predicted temperature profiles and velocity profiles at the boiler bank and superheater heat transfer surfaces were not affected significantly by these inlet conditions. Two turbulence models were used, the traditional k-ϵ model and an algebraic stress model. Differences in predicted results between turbulence models were minor.

General features of the simulated results agree well with field measurements. Recirculation zones were located above the protruding edge of the bullnose and in the uppermost corner of the upper furnace cavity. The degree to which the bullnose protruded into the furnace had a significant effect on the size of recirculation above the bullnose. A smaller bullnose results in a smaller recirculation zone which results in smoother superheater tube temperature profiles.

INTRODUCTION

Recovery of the pulping chemicals and the chemical energy in dissolved lignin is important to the economic viability of the kraft pulping process. Recovery boilers are specifically designed to carry out both of these tasks. A number of factors may limit the maximum capacity of these units and make increased capacity difficult to achieve and maintain. Pluggage of the convective section of these boilers by low-melting-point solids escaping the lower furnace is one of the most common capacity constraints on Kraft recovery boilers.

The solid material which can deposit on the superheater and boiler bank tubes and cause pluggage is derived both from submicron sodium fume volatilized in the combustion zone and by mechanical carry-over of burning black liquor droplets(1). In either case it is the low melting temperatures of the mixtures of sodium compounds which compose these solids that lead to deposition and hardening of material on the tubes in the superheater and boiler bank. The melting temperatures of the fume and carry-over lie between the gas temperature and the tube metal temperature existing throughout most of this region. This allows the carry-over and fume to be molten or partially molten in flight, but solid when in contact with a tube.

The melting characteristics of fume and carry-over materials in Kraft recovery boilers have been extensively studied(2-5). Less well studied are the gas temperatures and flow patterns in this region of the boiler. These profiles are important not only because of the impact on pluggage behavior, but also for corrosion behavior of the superheater tubes and efficient utilization of the tubes in the superheater and boiler bank for heat transfer and steam production.

There are few published studies which specifically address the gas flow and temperature profiles in the convective section of recovery boilers (6,7,8). Direct measurement of gas velocity and temperature in this region of recovery boilers is extremely difficult. High concentrations of semimolten solid material and complex flow patterns make direct measurement of gas velocity nearly impossible. Temperature measurement is somewhat easier, but very limited access for probes into this region make comprehensive investigation of gas temperature profiles time consuming, expensive, and uncertain. The difficulty of direct measurement on operating recovery boilers suggests the use of physical or mathematical models. Previous work (6,7,8) has been enlightening and encouraged more detailed investigation with a commercially available Computational Fluids Dynamics (CFD) computer code.

CFD codes are now being developed and used to investigate many aspects of the complex flow patterns of recovery boilers (9-15). Modeling the gas flow patterns and black liquor combustion in a recovery furnace is an extremely challenging task. However, commercial CFD codes are available which can reasonably model the less challenging flows associated with the convective section of recovery boilers. This region is characterized as one with a single inlet and exit, no significant chemical reaction and heat release, entrained condensed-phase material which does not significantly impact the gas flow, and, when the sootblowers are inactive, no small localized high velocity jets. This greatly simplifies CFD investigation of this region. The code used in this work was FLUENT v3.02 from Fluent, Inc., Lebanon, N.H. It was run on an IBM RISC Workstation Model 6540.

In any CFD model investigation, there are necessarily many assumptions and limitations on the predicted results. The size of grid elements and the suitability of their layout for the selected geometry being investigated is an uncertainty with all CFD investigations. The accuracy of the mathematical description of turbulence is another. More specific to the current investigation is the uncertainty in the inlet flow conditions to the region of interest. As will be discussed below under Model Description, approximately 50,000 computational nodes were used to investigate the flow in a vertical slab section of the boiler extending from below the bullnose to the economizer. A nonuniform grid spacing was used to maintain good resolution while minimizing the number of total nodes. A previous investigation (6) compared CFD predictions of gas flow patterns with isothermal physical model measurements. Satisfactory comparison between predictions and measurements when a similar node spacing was employed indicates that the current node spacing is adequate for the present investigation.

In the previous investigation (6), model results were compared for two different assumptions about the description of turbulence in the flow. One assumption was the widely used κ-ϵ model, the other a modified laminar viscosity model. In the present investigation, the predictions using the κ-ϵ model will be compared to a more complex description of turbulence, the so-called algebraic stress model, in order to assess the sensitivity of the predicted results to the turbulence description.

The inlet flow conditions to the region being modeled are those of the upper region of the recovery furnace. These flow conditions are generally not well known. They depend strongly on the geometry of the char bed and the number, layout, and velocity of the combustion air jets. The flow in the upper region of the furnace may contain the remnant of a channeled flow pattern, tangential swirling flow, and recirculation zones. These features can be very strong in the lower furnace near the air jets but dissipate somewhat due to turbulent shear in the upper furnace. Because the flow in the upper furnace is not well known, the impact of convective section "inlet" flow pattern on gas flow and temperature profiles was investigated by comparing two very different inlet conditions. These inlet conditions will be described below.

The remainder of this paper is broken into three sections. In the first section, a description of the convective section model is presented. The model geometry and physical parameters are presented along with a specification of the individual cases investigated. In the second section, the result of the CFD model predictions are discussed and comparisons among the cases are made. Finally, conclusions derived from the work are drawn.

Model Description

The tubes which comprise the superheater and boiler bank of a recovery furnace are generally vertical and always laid out in rows aligned with the gas flow path. The superheater tubes are frequently arranged as platens, closely spaced in-line tube bundles. This layout of recovery boiler convective tubes restricts crossflow and gives gas flow in this region a strongly two-dimensional nature. Because of this and the uniform side-to-side spacing of the 20 to 40 superheater platens which constitute a complete superheater section, a significant simplification of the flow model is possible. Instead of modeling the full side-to-side width of the boiler, only

a width equivalent to two side-to-side platen spacings is modeled. The actual region contains two superheater platens along with the gas lane between them and half a lane on either side. This region is shown as a shaded area in Figure 1. The region modeled extends from 7.5 m (24 ft) below the bullnose to the outlet of the first pass of the economizer. This gives a three-dimensional region which contains all the geometric features of the upper region of a recovery furnace, but is narrow enough to make effective use of 50,000 computational nodes.

One limitation of the physical model of a slab cut from the midsection of a boiler is the necessary assumption that there is little side-to-side, or rotational flow at the inlet plane of the model. The model predictions presented here would then not apply well to recovery boilers with tangential air systems.

The platens of the superheater were modeled as external wall cells with specified temperatures. Because of the grid structure, the platens are rectangular in view and are stairstep trapezoids in side elevation. The bullnose shape is also approximated by a stairstep profile. Because of the limited effect of boundary layer shear on these flows, only minor differences in overall flow pattern would be anticipated for this approximation of the relatively smooth bullnose shape. A side elevation of a vertical plane passing through the superheater platens is shown in Figure 2.

Heat transfer between the gas and the superheater and boiler bank surfaces depends on the gas temperature and surface temperature as well as the overall heat transfer coefficient. Both radiation and convection occur between the gas and the surfaces, and these heat transfer processes can be affected by gas and surface properties as well as the properties of the deposits which invariably cover these surfaces in a recovery boiler. Because the main emphasis of the present effort is to examine the influence of assumed inlet conditions, assumed turbulence model, and bullnose shape, both the surface temperature and overall heat transfer coefficient were simply specified for each section. The values for each section are given below in Table 1.

Table 1. Overall Heat Transfer Coefficients and Temperatures for Heat Transfer Surfaces.

Section	Heat Trans. Coeff. (Watts/M^2°C)	Temperature (°C)
1st Superheater Section	172	387
2nd Superheater Section	105	417
3rd Superheater Section	132	327
Boiler Bank	177	297

Gas properties required for the calculations are based on those for an ideal gas with a molecular weight similar to air.

All CFD codes attempt to provide a numerical solution of the Navier-Stokes equations and the energy equation. For turbulent flows, a description of the turbulent transport of energy and momentum is required. The well-known κ-ϵ model is often used, and its limitations and inaccuracies have been extensively studied in the literature by comparing CFD model predictions to measured results. This was done specifically for the convective section of a recovery boiler in a previous study (6). However, to further substantiate that the κ-ϵ model did not cause significant errors in the model results, an alternative, more complex turbulence model was also tried. This alternative model is the so-called algebraic-stress (ASM) model available as a standard option in the FLUENT code. Comparisons will be made below between the model results using the two turbulence models. Except as shown in this comparison all other CFD results were obtained using the standard κ-ϵ model for turbulence.

The flow profile entering the upper furnace region is not well known for any boiler configuration. However, there is good reason to believe that this profile does not significantly impact the flow profile in the convective section. This profile would only be important if the dynamic head due to the flow velocity was a substantial fraction of the actual pressure drop across the convective section of the boiler. The static pressure drop of the gas stream across the superheater section of a recovery boiler is approximately 0.2 inches of WC (50 Pa). The average upward gas velocity in the furnace is about 14 ft/s (4.3 m/s). The dynamic head is equal to one-half the product of the gas density (about 0.018 lbm/ft^3 or 0.28 kg/m^3) and the velocity squared or 0.01 inches of WC (2.6 Pa). This is quite low compared to typical pressure drops.

In order to further test the impact of inlet flow profile on the CFD model predictions, the results using profiles were compared. The first profile was uniform both in inlet velocity and inlet temperature. For comparison, a parabolic profile at the inlet was assumed. Comparisons of the inlet velocity and temperature profiles for the two assumptions for one firing rate are shown in Figures 3 and 4.

The main purpose of the study was to determine the effect of the bullnose size and shape on the gas flow patterns in the convective section of the boiler. Here, the size of the bullnose is indicated by the horizontal flow area in the region of the bullnose compared to that of the open furnace area. Typically, the ratio is about 50%. Three values were used in this study, 42% (small flow area, large bullnose), 52%, and 62% (large flow area, small bullnose). The shape of the bullnose can also be changed from relatively thin sloping to thick abrupt. In all, three different nose sizes (42%, 52%, 62%) and three nose shapes (sloping, intermediate, abrupt) were examined.

The general operating conditions used in this study were for a boiler firing black liquor at a rate of 14.2 kg/s dry solids (2.7 x 10^6 lbm/d) with a heating value of 14.2 MJ/kg (6100 BTU/lbm) in a furnace of 8.2 m x 8.2 m (27 ft. x 27 ft.) cross section. This yields an average upward gas velocity of 5.1 m/s (16.7 ft/s). For comparison, some runs were carried out at 4.1 m/s (13.5 ft/s). The average gas temperature at the inlet to the region being modeled was taken

at 1350°K (1077°C or 1970°F). The base case conditions are intended to correspond approximately to a heavily loaded recovery boiler.

Using the current version of the FLUENT code and configuration of the computer, each case required approximately 24 hours to converge to a point where the sum of all residuals was less than 10^{-4}.

RESULTS AND DISCUSSION

All CFD computations are characterized by voluminous output, values of temperature, pressure, all three components of velocity, and turbulence parameters at each node. For the present calculations with approximately 50,000 nodes this amounts to almost 350,000 numbers. Graphical presentation is mandatory and fortunately the flows in the present cases are predominantly two-dimensional. Both vector velocities and velocity contours will first be presented for the base case and then comparisons will be made with other cases.

The base case consists of uniform velocity and temperature profiles at the inlet, an intermediate 52% bullnose, and the κ-ϵ turbulence model. Shown in Figure 5 is a plot of the velocity contours along the center plane between the two superheater platens. Shown in Figure 6 are the corresponding temperature contours. The velocity contours indicate that the flow accelerates as it approaches the bullnose, then rises well above the bullnose before turning toward the boiler bank. A recirculation zone can be seen along the top surface of the bullnose. There is another small recirculation zone in the upper left-hand corner of the upper furnace cavity, but accurate prediction in this region would not be expected due to the low density of computational nodes in this vicinity. The tightly spaced contour lines immediately in front of and parallel to the boiler bank are due to acceleration of the gas flow in the region of the more tightly spaced boiler bank.

The temperature contours show a more consistent steady decrease in gas temperature as it passes through the convective system to the economizer. The influence of the recirculation zone above the bullnose can be seen on the temperature contours.

Two similar cases were run to investigate the influence of the turbulence model on the predicted flow and temperature patterns. The two cases both used a uniform inlet temperature but a parabolic inlet velocity profile. A direct comparison of the profiles predicted for the two turbulence models is shown in Figure 7, and a similar comparison for the temperature profiles is shown in Figure 8. In both cases the flows and temperature are very similar. Only very minor detailed difference could be found by overlaying the plots for the ASM turbulence model and the κ-ϵ turbulence model. Convergence for the ASM model was much more difficult, taking nearly 10 times as long to converge as the case with the κ-ϵ model. This indicates that for these particular flows there is little accuracy benefit from the use of a turbulence model other than the κ-ϵ model, and there is a severe penalty in convergence time. All other cases in this study were carried out with the κ-ϵ turbulence model.

Shown in Figure 9 are velocity plots for four cases: 1) uniform inlet velocity and inlet temperature, 2) parabolic velocity and uniform temperature, 3) uniform velocity and parabolic temperature, and 4) parabolic velocity and temperature. Figure 10 shows corresponding plots for temperature. There are some differences between the profiles, but the very large differences depicted in Figures 3 and 4 for the inlet parabolic profiles are strongly attenuated as the gases pass through the convective section. This is particularly obvious for the velocity at the boiler bank inlet. For the temperature profiles, the 200°C (360°F) difference in inlet temperature between the uniform and parabolic profile is attenuated to only 40°C (72°) at the boiler bank.

The relative insensitivity of the predicted results indicates that uncertainty in the inlet profile should not affect the relative importance of other design parameters on convective section performance. Advantage will be taken of this for the comparison of the influence of bullnose size and shape on flow and temperature profiles.

The effect of bullnose size has been investigated for three sizes. The bullnose restricts the flow area, so the bullnose size has been specified in terms of the horizontal open gas flow area at the bullnose tip compared to the plan area of the open furnace. A large bullnose with 42% open flow area has been compared to a medium bullnose with 52% and a small bullnose with 62% open flow area. Each of these cases was run with 5.1 m/s (16.7 ft/s) uniform inlet gas velocity and 1350°K (1077°C or 1970°F) uniform inlet gas temperature. The velocity and temperature contours for the 52% bullnose case were previously presented in Figures 5 and 6. Shown in Figure 11 is a comparison of the velocity contours for the 42% (large bullnose) and 62% (small bullnose) cases. Shown in Figure 12 is the corresponding comparison of the temperature contours.

In both figures it is readily apparent that the larger bullnose (42% case) causes higher upward gas velocity at the bullnose, and this results in significant penetration of the flow into the open cavity in front of the superheater. Flow through the superheater in the 42% case is substantially horizontal, and there is a much larger recirculation zone above the bullnose. Vertical temperature gradients are much higher for the 42% (large bullnose) case. This would lead to poor utilization of the superheater heat transfer surface and potentially higher deposition and corrosion. Considering that the purpose of the large bullnose is to protect the superheater tubes from radiation from the lower furnace, it is clear that selection of bullnose size is very much a trade-off between radiation protection and convective heat transfer surface utilization.

The shape of the bullnose can be changed by changing the angle of the upstream face of the bullnose. Three cases were run to investigate the influence of bullnose shape. The base case discussed above had an upstream face angled into the flow at about 45°. A second shape was used which was more abrupt, at an angle of nearly 75°. A third had a sloping nose which also had a slight curve inward to an angle of about 25°. All three cases were run at 5.1 m/s (16.7 ft/s) uniform inlet gas velocity, 1350°K (1077°C or 1970°F) uniform inlet gas temperature, and a 52% open flow area bullnose size.

Shown in Figure 13 are the velocity contours for all three bullnose shapes. The shape of the bullnose is apparent in this figure as is the reason for calling the 75°angle bullnose an abrupt bullnose and the 25° angle a sloping bullnose. The corresponding temperature contours for all three cases are shown in Figure 14.

There are some significant differences between the gas flow contours for these bullnose shapes. This is easiest to see by comparing the size of the recirculation zone above the bullnose. It is larger for the abrupt bullnose than for the sloping bullnose. Likewise, the gas flow through the superheater is more horizontal for the abrupt bullnose, leading to poorer utilization of the heat transfer surface because less is exposed to the main gas flow. This is a situation where the same protection from lower furnace radiation is provided by all three bullnoses, but convective heat transfer utilization is significantly different depending on the abruptness of the upstream face.

The predicted effect of the bullnose shape on the recirculation zone and gas flow can be readily understood by reference to ordinary nozzle flow. The restriction at the bullnose elevation is similar to that for flow through a nozzle or orifice. A smooth approach to the restriction such as the sloping bullnose is similar to a flow nozzle. The abrupt bullnose looks more like a sharp-edged orifice. Well-documented flow patterns for the sharp-edged orifice show that there is a contraction of flow down-stream from the physical orifice. For a smooth flow nozzle, the minimum flow area is at the nozzle itself. Thus, for the same flow and same physical open area, the flow is slower and more uniform for the smooth flow nozzle. This is just the case for the convective section flows shown in Figures 13 and 14. The abrupt bullnose causes higher upward velocities, greater penetration of the flow into the upper furnace cavity, and a larger recirculation zone above the bullnose.

CONCLUSIONS

A commercially available CFD code has been used to investigate the flow and temperature profiles in the convective section of a recovery boiler. The uncertainty in the inlet gas flow conditions and the mathematical description of turbulent flows were first investigated. Comparison of the assumption of uniform inlet gas flows to sharply parabolic inlet flows showed that the predicted results for velocity and temperature were insensitive to the precise inlet flow condition. This is reasonable in light of the relatively low initial dynamic head of the upward furnace gas flow. Likewise, comparison of two models for the description of turbulence showed very little impact on the predicted results. As a result, the familiar κ-ϵ model for turbulence was selected for most of the study due to its near factor of 10 more rapid convergences.

The effect of the size and shape of the bullnose on gas temperature and velocity was investigated for three sizes and three shapes. Both the size and shape affected the gas flow. The magnitude and direction of the effects can be easily rationalized in terms of the effect of shape and size on gas velocity in the bullnose region and penetration of the gas flow into the upper furnace cavity.

ACKNOWLEDGEMENT

Funding for this project was provided by the U.S. Department of Energy under contract DE-FG02-90CE40936.

One of the authors, Esa K. Vakkilainen, received boiler specifications for the cases run in this study from the Ahlstrom Company. This assistance is greatly acknowledged.

REFERENCES

1. Tran, H.N., "How Recovery Boilers Become Plugged," TAPPI Kraft Rec. Op. Seminar, Orlando, FL, January 1992.

2. Reeve, D.W., Tran, H.N., and Barham, D., Pulp & Paper Canada, 82(9):T315-T320 (1981).

3. Tran, H.N., TAPPI J. 69(11):102 (1981).

4. Backman, R., Hupa, M., and Uppstu, E., TAPPI J. 70(6):123-127 (1987).

5. Tran, H.N., Barham, D., and Reeve, D.W., TAPPI J. 71(4):109 (1988).

6. Vakkilainen, E.K., Nikkanen, S., Hautamaa, J., and Anttonen, T., "Flows in the Upper Region of Recovery Boilers," AIChE Annual Mtg., Los Angeles, November 1991.

7. Haynes, J.B., Adams, T.N., and Edwards, L.L., TAPPI J. 71(9):81 (1988).

8. Chapman, P.J., Janik, S.G., and Jones, A.K., Tappi Eng. Conf. Proc., Nashville, September 1991.

9. Grace, T., Walsh, A., Jones, A., Sumnicht, D., and Farrington, T., "Three-Dimensional Mathematical Model of the Kraft Recovery Furnace," CPPA/TAPPI Int. Chem. Rec. Conf., Ottawa, April 1989.

10. Walsh, A.R., "A Computer Model for In-Flight Black Liquor Combustion in a Kraft Recovery Furnace," Ph.D. Thesis, IPC, January 1989.

11. Jones, A.K., "A Model of the Kraft Recovery Furnace," Ph.D. Thesis, IPC, January 1989.

12. Sumnicht, D.W., "A Computer Model of a Kraft Char Bed," Ph.D. Thesis, IPC, April 1989.

13. Karvinen, R., Hyoty, P., and Siiskonen, P., Tappi J. 74(12):171-177 (1991).

14. Chapman, P.J., and Jones, A.K., Tappi J. 75(3):133-137 (1992).

15. Salcudean, M., Gartshore, I., Abdullah, Z., Nowak, P., Aghdasi, F., Quick, J., and Tse, D., Annual Report to U.S. DOE for Contract No. DE-FG02-90CE40936, September 1991.

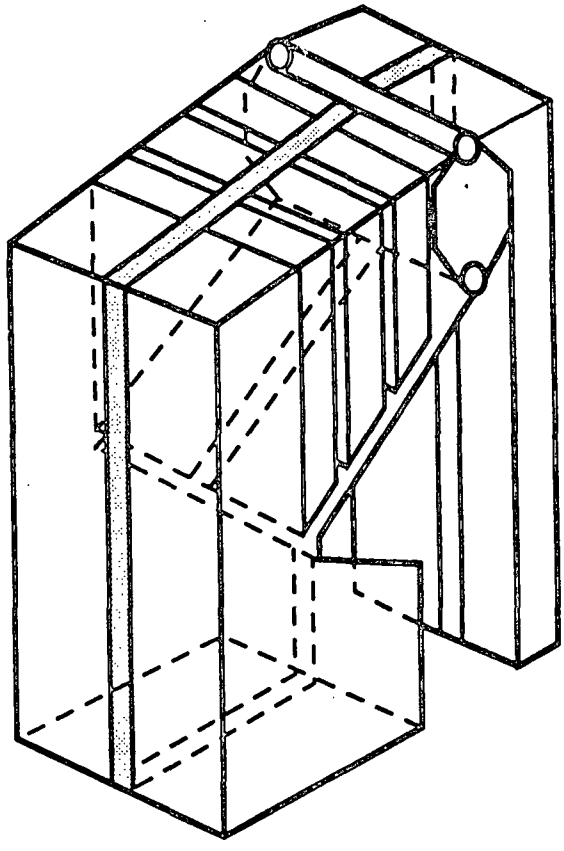

Figure 1. View of a Vertical Slice Through the Convective Section of a Recovery Furnace.

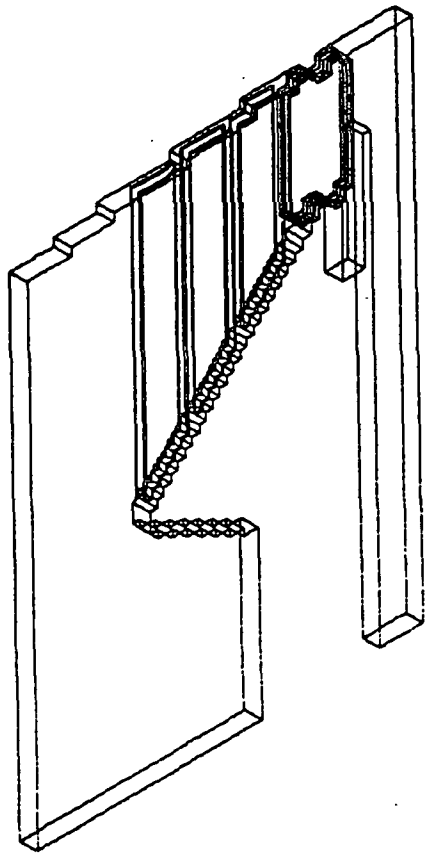

Figure 2. Side View of CFD Problem Boundaries.

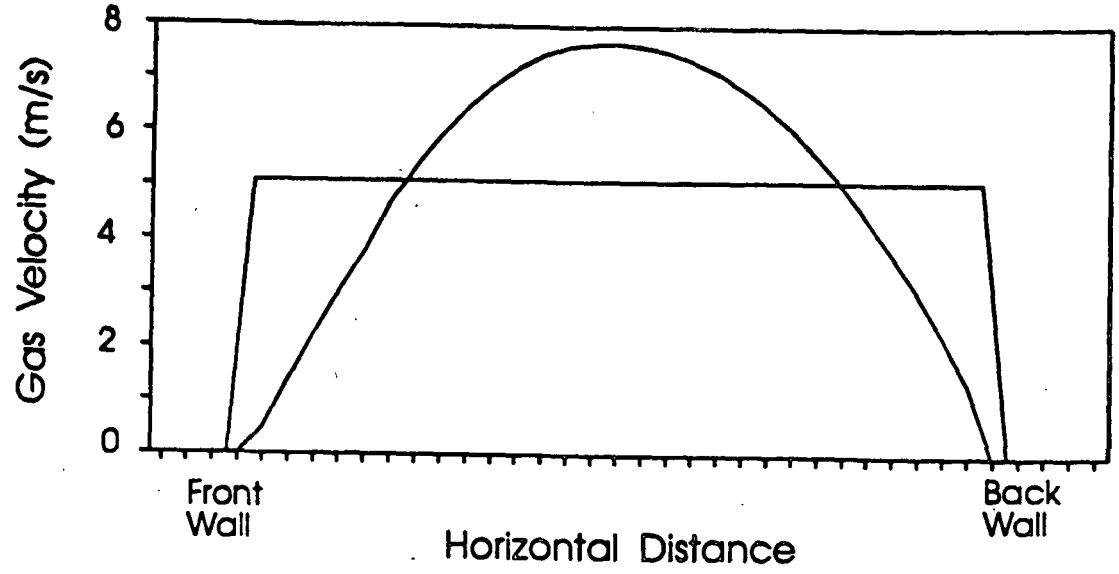

Figure 3. Uniform and Parabolic Inlet Velocity Profiles.

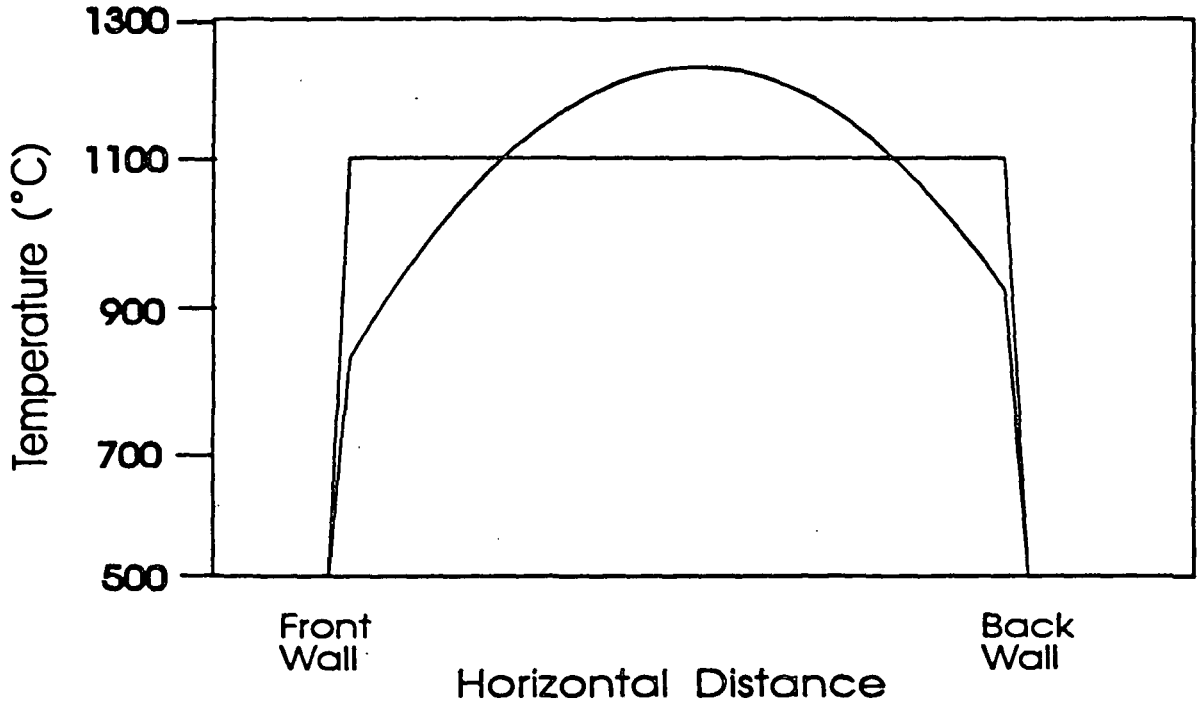

Figure 4. Uniform and Parabolic Inlet Temperature Profiles.

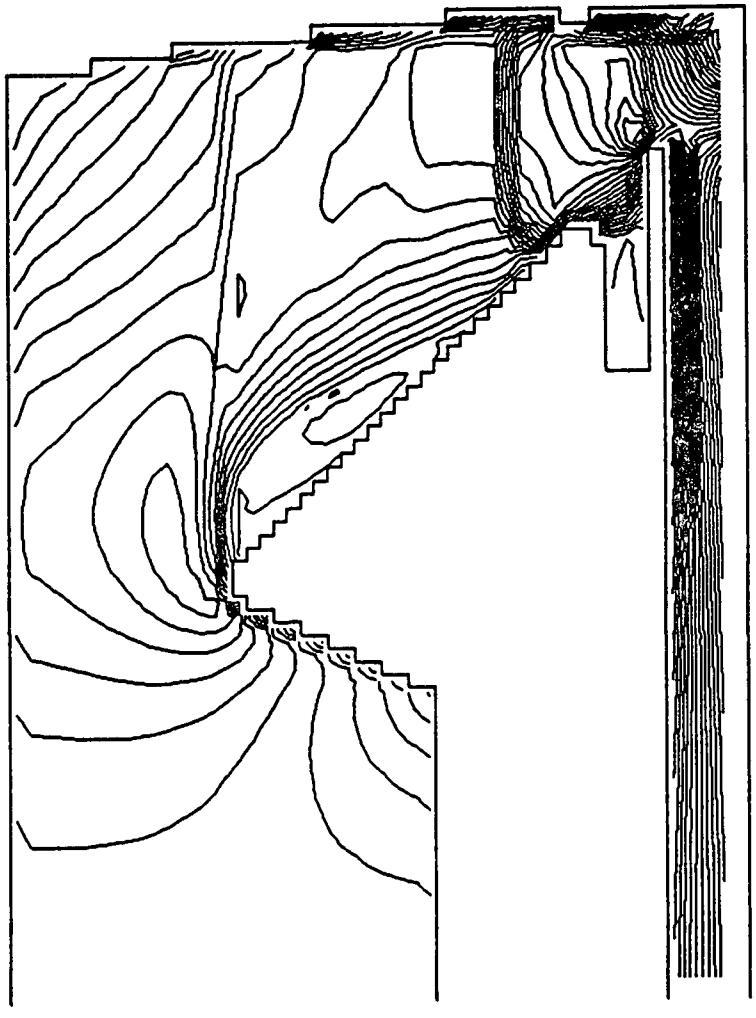

Figure 5. Velocity Contours for the Base Case Simulation with Intermediate Bullnose Size (52% Open Flow Area).

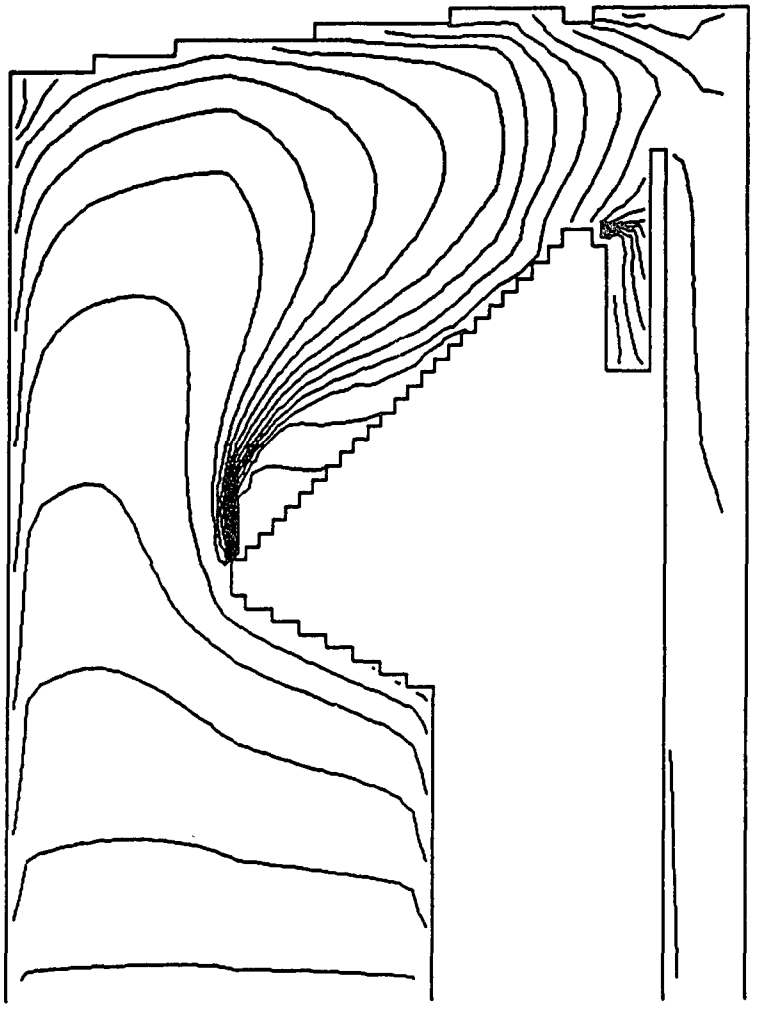

Figure 6. Temperature Contours for the Base Case Simulation with Intermediate Bullnose Size (52% Open Flow Area).

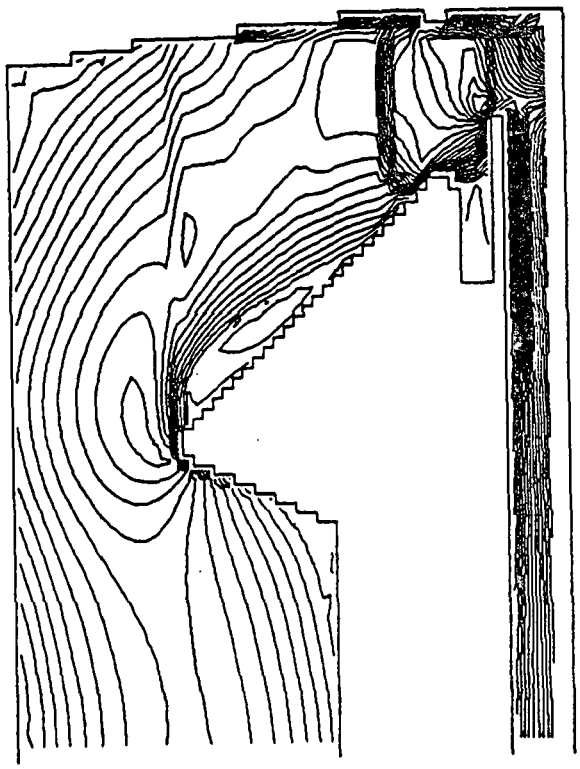

a) k-ε Turbulence Model

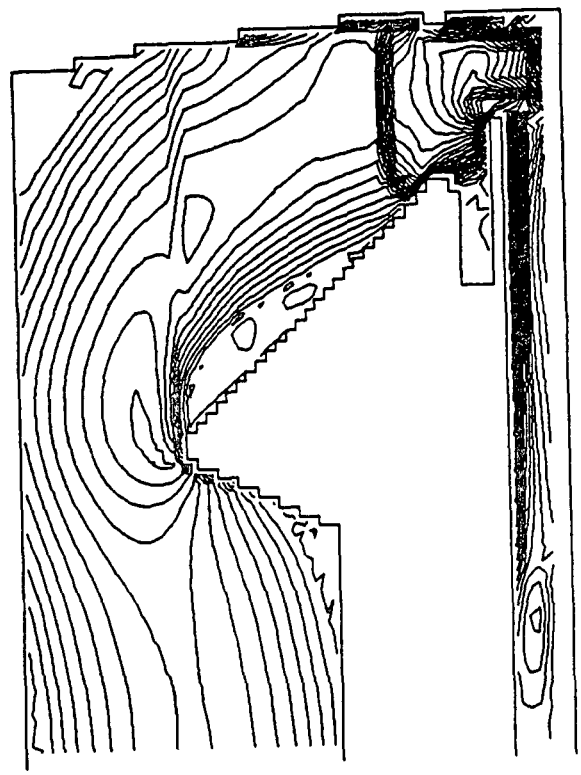

b) ASM Turbulence Model

Figure 7. Velocity Magnitude Contours for Two Turbulence Models.

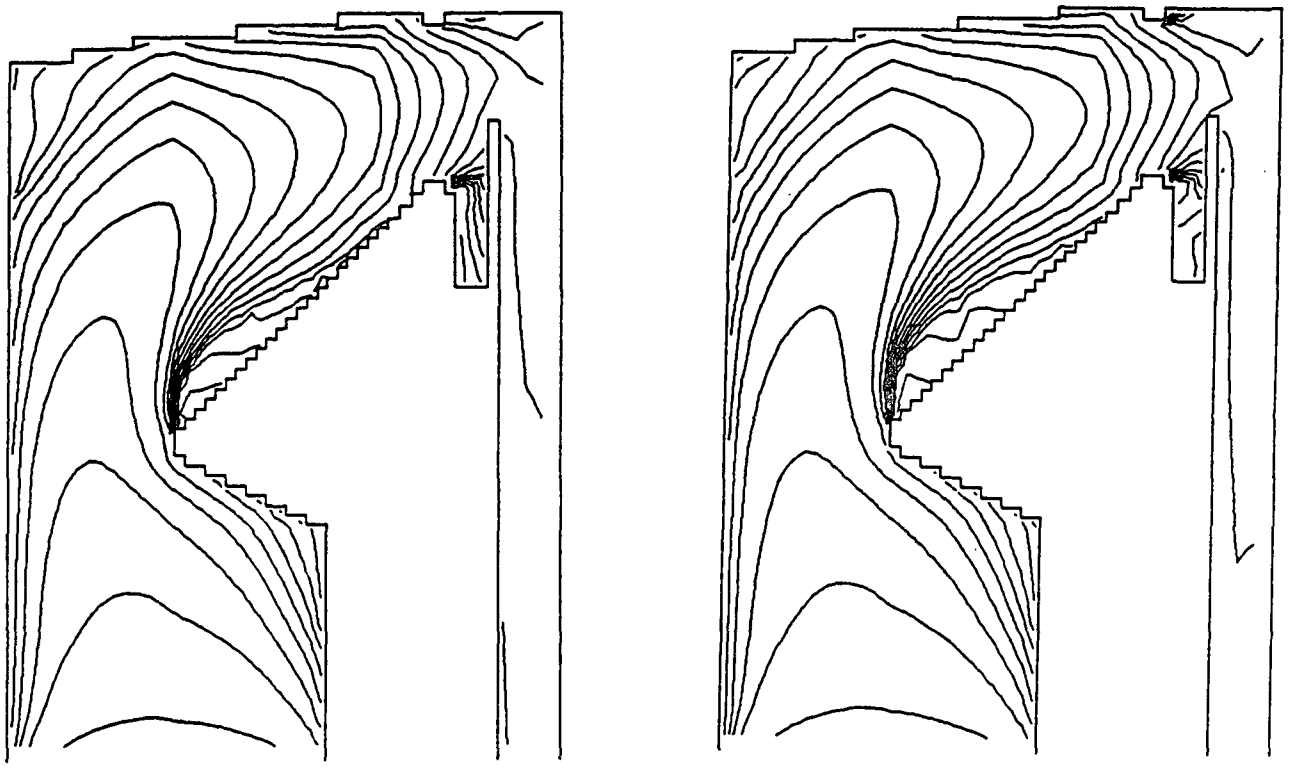

a) k-ϵ Turbulence Model

b) ASM Turbulence Model

Figure 8. Temperature Contours for Two Turbulence Models.

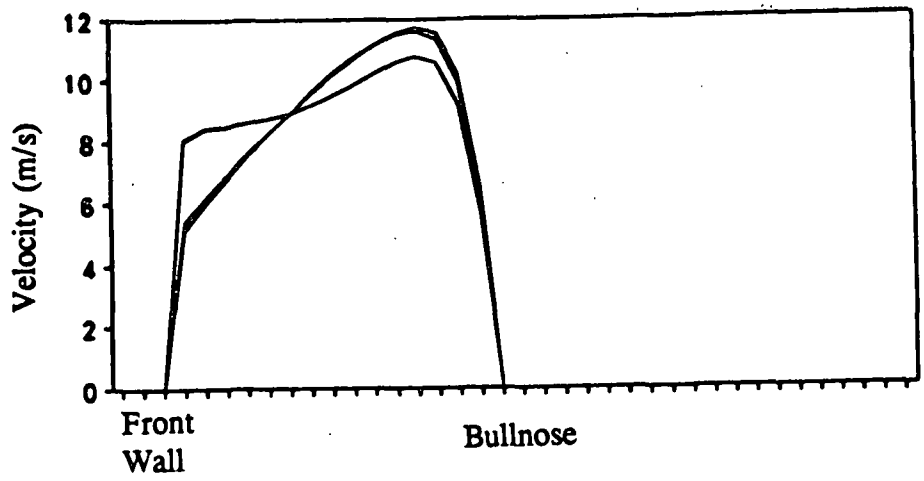

a) Velocity Profiles at the Bullnose

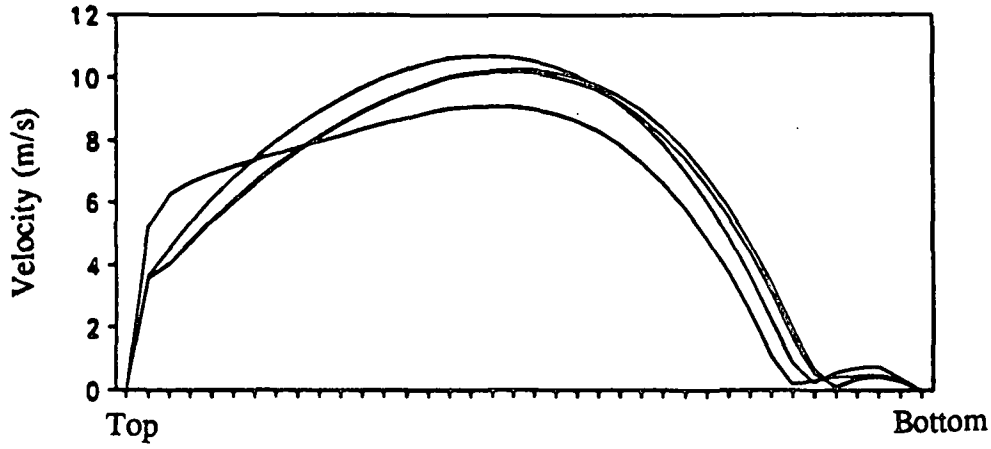

b) Velocity Profiles at the First Superheater Section

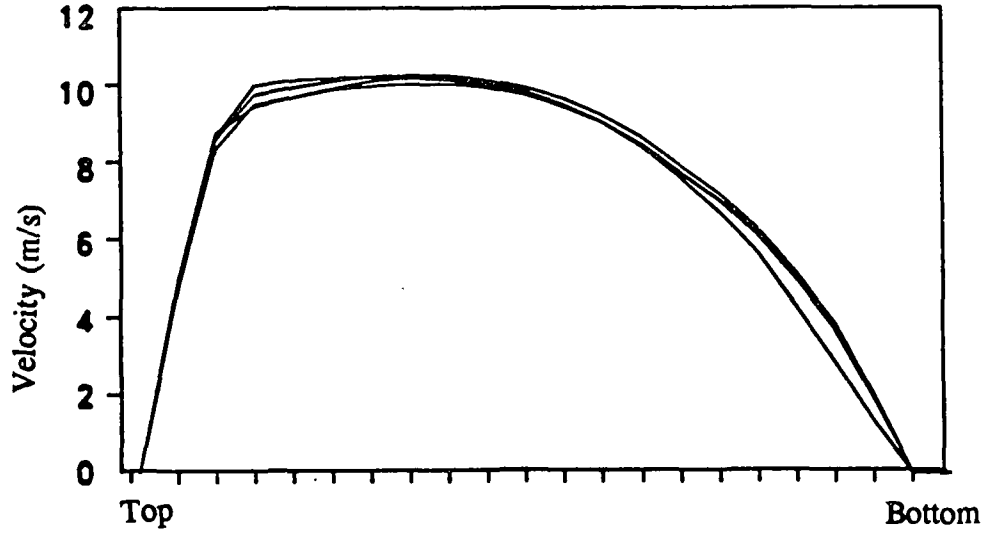

c) Velocity Profiles at the Boiler Bank

Figure 9. Velocity Profiles for Four Cases at Three Locations.

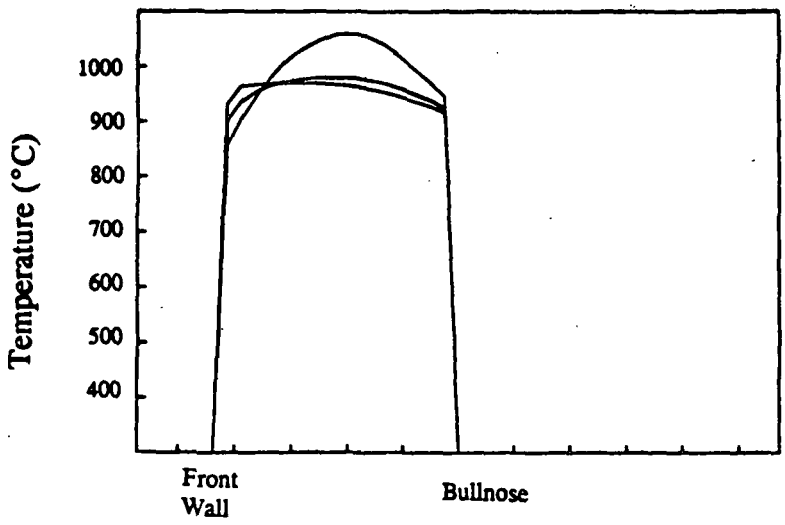

a) Temperature Profiles at the Bullnose

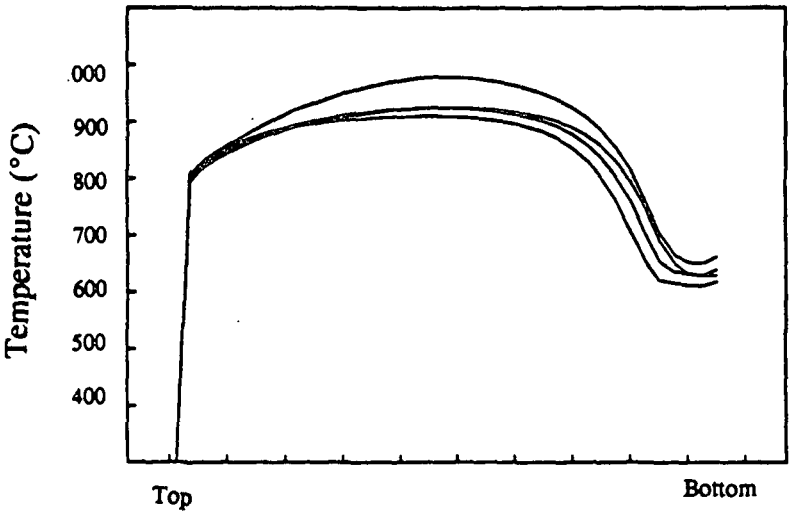

b) Temperature Profiles at the First Superheater Section

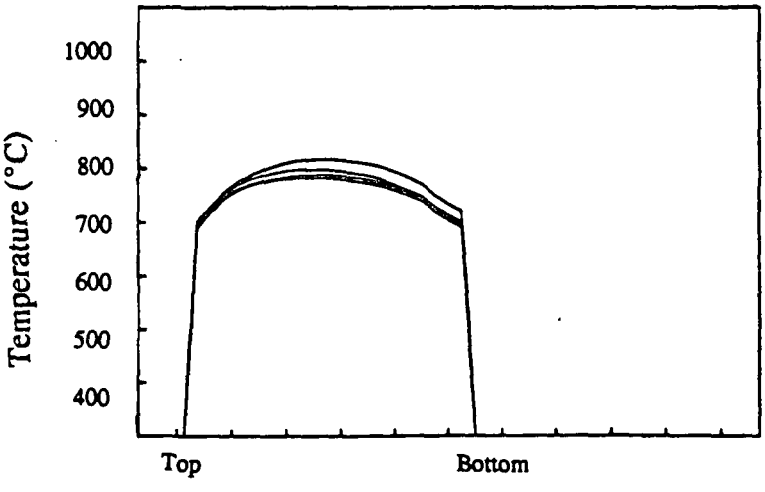

c) Temperature Profiles at the Boiler Bank

Figure 10. Temperature Profiles for Four Cases at Three Locations.

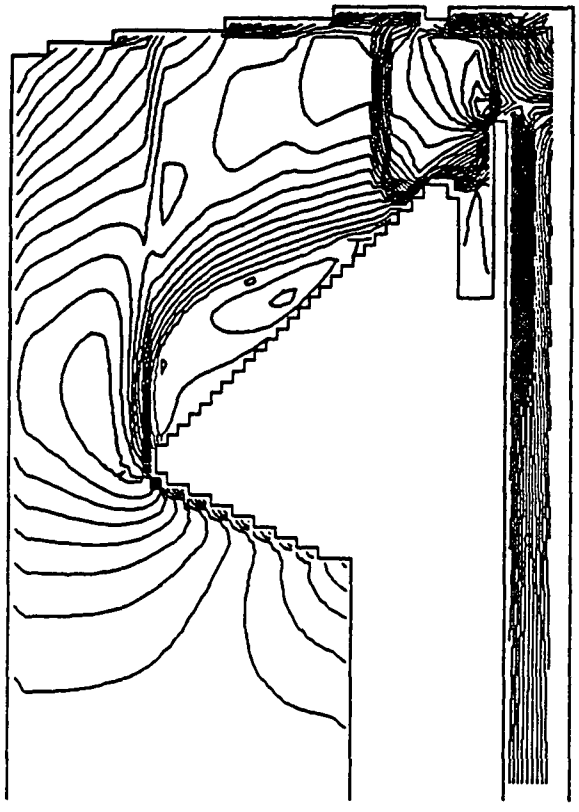

a) Velocity Contours for Large Bullnose

(42% Open Flow Area)

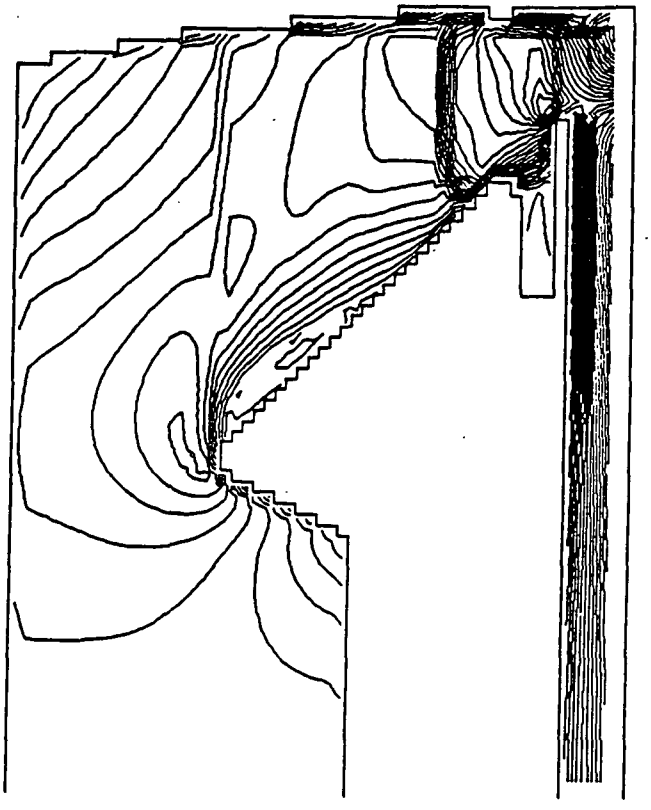

b) Velocity Contours for Small Bullnose

(62% Open Flow Area)

Figure 11. Velocity Contours for Large and Small Bullnose Sizes.

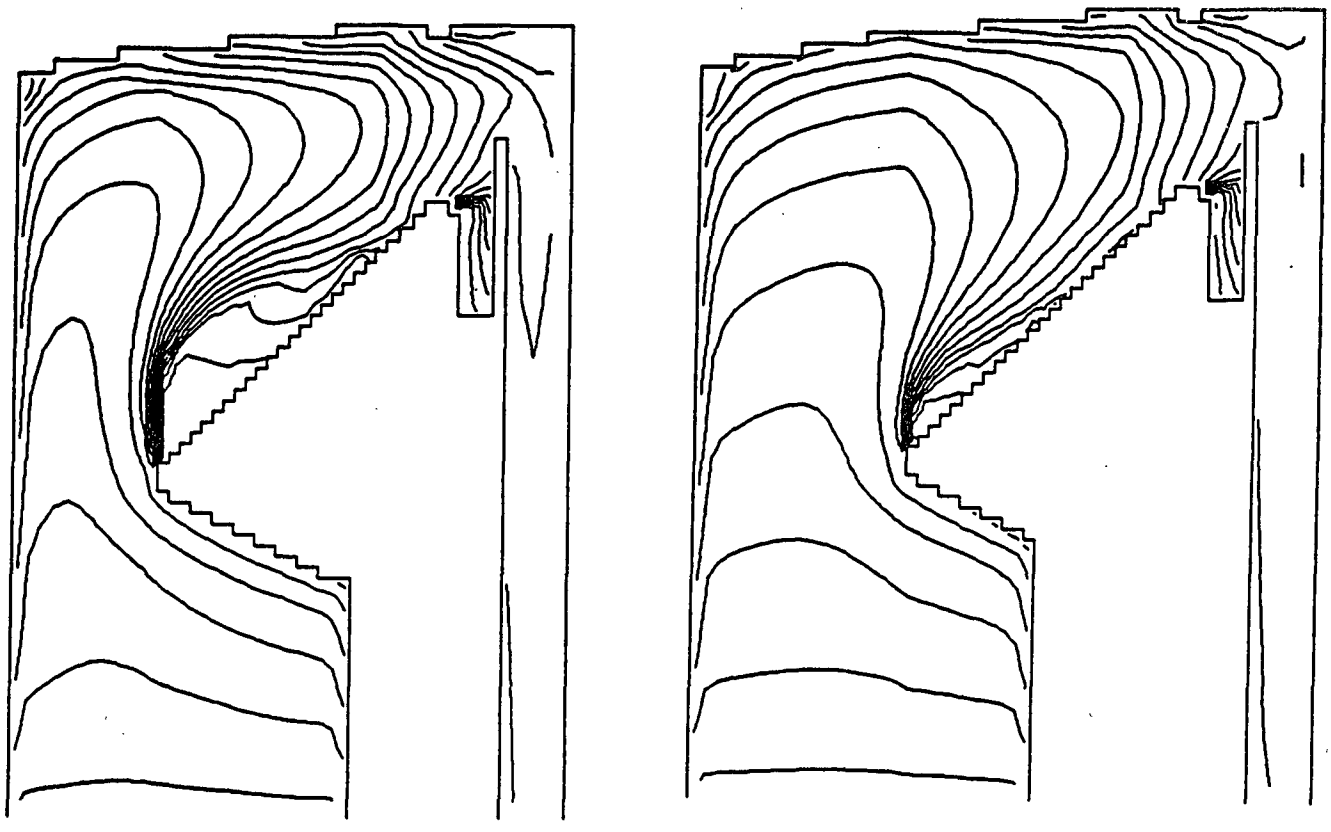

a) Temperature Contours for Large Bullnose (42% Open Flow Area)

b) Temperature Contours for Small Bullnose (62% Open Flow Area)

Figure 12. Temperature Contours for Large and Small Bullnose Sizes.

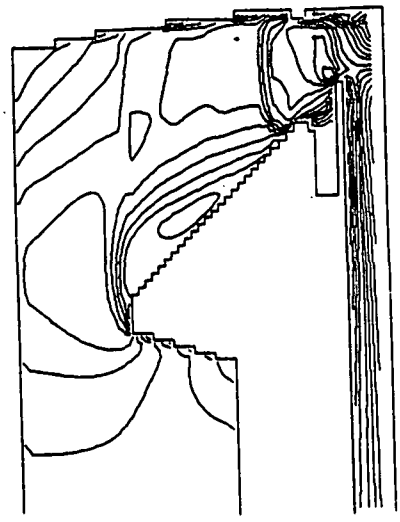

a) Velocity Contours for an Abrupt Bullnose

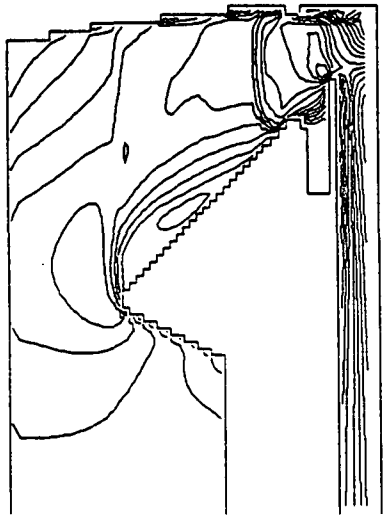

b) Velocity Contours for an Intermediate Bullnose

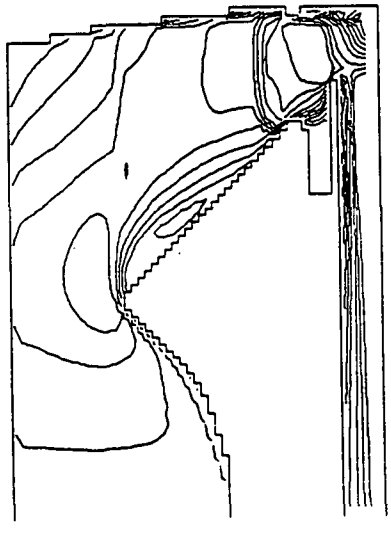

c) Velocity Contours for a Sloping Bullnose

Figure 13. Velocity Contours for Three Bullnose Shapes.

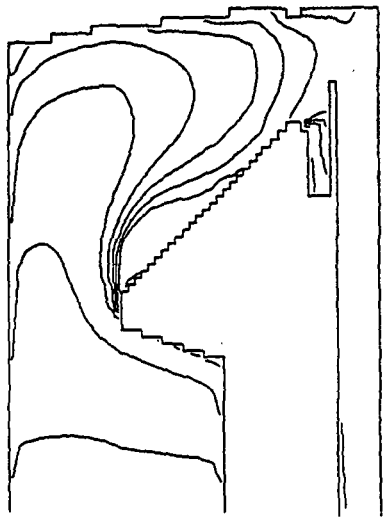

a) Temperature Contours for an Abrupt Bullnose

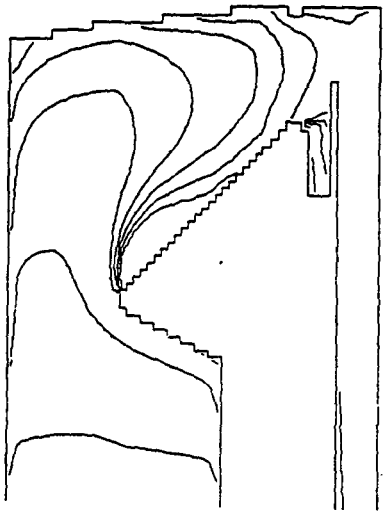

b) Temperature Contours for an Intermediate Bullnose

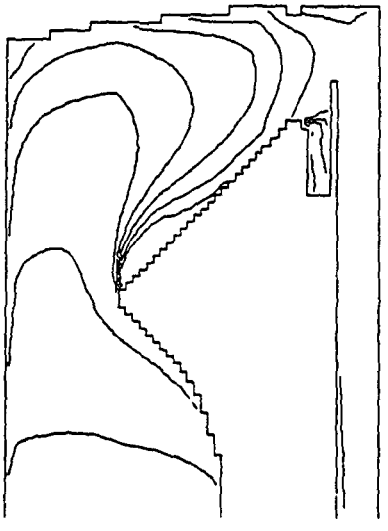

c) Temperature Contours for a Sloping Bullnose

Figure 14. Temperature Contours for Three Bullnose Shapes.